Document downloaded from:

http://hdl.handle.net/10251/84548

This paper must be cited as:

Martínez Casas, J.; Giner Navarro, J.; Baeza González, LM.; Denia Guzmán, FD. (2017). Improved railway wheelset-track interaction model in the high-frequency domain. Journal of Computational and Applied Mathematics. 309(1):642-653. doi:10.1016/j.cam.2016.04.034.

The final publication is available at

http://dx.doi.org/10.1016/j.cam.2016.04.034

Copyright Elsevier

Additional Information

Accepted Manuscript

Improved railway wheelset-track interaction model in the high-frequency domain

José Martínez-Casas, Juan Giner-Navarro, L. Baeza, F.D. Denia

PII: S0377-0427(16)30214-X
DOI: http://dx.doi.org/10.1016/j.cam.2016.04.034
Reference: CAM 10627

To appear in: *Journal of Computational and Applied Mathematics*

Received date: 30 November 2015
Revised date: 22 April 2016

Please cite this article as: J. Martínez-Casas, J. Giner-Navarro, L. Baeza, F.D. Denia, Improved railway wheelset-track interaction model in the high-frequency domain, *Journal of Computational and Applied Mathematics* (2016), http://dx.doi.org/10.1016/j.cam.2016.04.034

This is a PDF file of an unedited manuscript that has been accepted for publication. As a service to our customers we are providing this early version of the manuscript. The manuscript will undergo copyediting, typesetting, and review of the resulting proof before it is published in its final form. Please note that during the production process errors may be discovered which could affect the content, and all legal disclaimers that apply to the journal pertain.

ACCEPTED MANUSCRIPT

HIGHLIGHTS

- *3D Moving Element Method (MEM) to model the track is proposed.*
- *The model considers an Eulerian coordinate system attached to the moving vehicle.*
- *The resulting formulation permits to reduce the computational cost compared to the FE models commonly used.*
- *The proposed 3D MEM track model is suitable to describe the high frequency dynamics.*

ACCEPTED MANUSCRIPT

Manuscript
Click here to view linked References

ACCEPTED MANUSCRIPT

Improved railway wheelset-track interaction model in the high-frequency domain

Authors: José Martínez-Casas[1*], Juan Giner-Navarro[1], L. Baeza[1] and F. D. Denia[1]

Affiliation:

[1]Centro de Investigación en Ingeniería Mecánica, Universitat Politècnica de València, Camino de Vera s/n, 46022 Valencia, Spain.

* Corresponding author

E-mail corresponding author: jomarc12@mcm.upv.es

Short title: Wheelset-track interaction in high-frequency domain

Address for correspondence:

José Martínez-Casas
Centro de Investigación en Ingeniería Mecánica.
Universitat Politècnica de València.
Camino de Vera s.n.,
46022 Valencia.
Spain.
Tl: +34 963877007, Ext. 76267
Fax: +34 963877629
e-mail: *jomarc12@mcm.upv.es*

ACCEPTED MANUSCRIPT

ACCEPTED MANUSCRIPT

ABSTRACT

As it is well known, there are various phenomena related to railway train-track interaction, some of them caused by the high frequency dynamics of the system, such as rolling noise when the vehicle runs over the track, as well as squeal noise and short-pitch rail corrugation for curved tracks. Due to these phenomena and some others unsolved so far, a large effort has been made over the last 40 years in order to define suitable models to study the train-track interaction. The introduction of flexibility in wheelset and rail models was required to have a more realistic representation of the wheel-rail interaction effects at high frequencies. In recently published train-track interaction models, the rails are modelled by means of Timoshenko beam elements, valid up to 1.5 kHz for lateral rail vibration and up to 2 kHz for vertical vibration. This confines the frequency range of validity for the complete train-track model to 1.5 kHz.

With the purpose of extending the range of validity above 1.5 kHz, a 3D track model based on the Moving Element Method (MEM) is developed in this paper to replace the Timoshenko beam considered in earlier studies, adopting cyclic boundary conditions and Eulerian coordinates. The MEM approach considers a mobile Finite Element (FE) mesh which moves with the vehicle, so the mass of the rail 'flows' with the vehicle speed but in the opposite direction through the mesh. Therefore, the MEM permits to fix the contact area in the middle of a finitely long track and to refine the mesh only around the contact area, where the forces and displacements will be more significant. Additionally, a modal approach is adopted in order to reduce the number of degrees of freedom of the rail model. Both strategies lower substantially the computational cost. Simulation results are presented and discussed for different excitation sources including random rail roughness and singularities such as wheel flats. All the simulation cases are carried out for a Timoshenko beam and a 3D MEM track model in order to point out the differences in the contact forces above the range of validity of the Timoshenko

ACCEPTED MANUSCRIPT

beam.

Keywords

Flexible wheelset; flexible track; moving element method; train-track interaction; high frequency dynamics.

ACCEPTED MANUSCRIPT

ACCEPTED MANUSCRIPT

1. INTRODUCTION

The complexity of the train-track interaction comes from the vibration coupling between the railway vehicle and the track, in which wheel-rail contact forces couple both sub-systems and their surface imperfections, such as rail roughness and wheel out-of-roundness, excite the global system. Unwanted phenomena such as damage of the rolling surfaces in the form of high levels of noise and vibration [1], corrugation [2], wheelset axle fatigue [3] and stress damage may appear in some cases due to large levels of vibration and dynamic fluctuations of the contact forces.

Many suitable train-track interaction models have been developed over the last 40 years, incorporating more recently flexibility in the wheelset in order to widen the frequency range of analysis [1,4]. Finite Element (FE) models have strongly entered in railways research to extend the frequency range above 1 kHz to address the rolling noise phenomenon [5,6] and, only very recently, further works have considered the inertial effects due to wheelset rotation running on a tangent [3] and curved track [7].

Historically, a frequency domain approach has been used to address the moving load problem by means of the Fourier Transform Method (FTM) and a moving coordinate system. Mathews [8,9] considered an arbitrary load moving along an infinite beam resting on an elastic foundation and solved the problem by using FTM. Jézéquel [10] utilised the same methodology for an Euler-Bernoulli infinite beam (considering the rotational and transverse stiffness) with a Winkler foundation subjected to a concentrated force moving with constant speed. Other extended focus [11] is based on a time domain approach based on Timoshenko flexible beam model which considers a simply supported infinite beam subjected to moving loads.

ACCEPTED MANUSCRIPT

These mentioned works consider rail beams as continuum and solve the equation of motion through an analytical approach. This makes them inappropriate when replacing a moving load by a complete moving vehicle system of massive number of degrees of freedom; for instance, the Timoshenko beam is only valid up to 1.5 kHz for lateral rail vibration and up to 2 kHz for vertical vibration [1]. Therefore, researchers have widely been using the well-known Finite Element Method (FEM), which physically discretises the track into a finite number of elements. Numerical time-stepping integrators are needed to solve the resulting equations of motion after assembling the element matrices. The FEM permits to extend the range of validity above the previous limit of 1.5 kHz and allows hence the complete wheelset-track model to comprise high frequency dynamic phenomena.

While considering a fixed global coordinate system in the FEM, the vehicle moves along the elements with time, thus the load vector has to be updated at each time step of the integration scheme. Additionally, there is the need of truncating the infinitely long track into a finite one with two corresponding artificial boundary ends, but the vehicle is moving forwards to the 'downstream' side. Therefore, the rail length required for reasonable simulation time-spans (without the vehicle exceeding the 'downstream' end), while preserving the refinement of the mesh, leads to an unapproachable number of degrees of freedom in the FEM.

To overcome both problems, Koh *et al.* [12] presented a formulation called Moving Element Method (MEM) based on an Eulerian coordinate system attached to the moving vehicle, instead of a fixed coordinate system. This method was initially adopted for a finite Euler-Bernoulli beam (1D). A new class of finite elements associated with the moving coordinate system is defined. Hence, the mesh is moving with this mobile frame and consequently the material of the rail 'flows' into this mesh. Another way to look at it is that these conceptual (not physical) elements 'flow' through the rail with the moving vehicle. This relative motion requires

ACCEPTED MANUSCRIPT

considering the material derivative for the formulation of the rail dynamics. The concept was afterwards extended to 2D moving elements in order to study moving load on continuum [13].

The novelty of the present article is the extension of the MEM concept to a tangent 3D track extruded from the UIC60 profile, adopting a FE technique and introducing cyclic boundary conditions [14]. The new methodology is herein referred to as the 3D Moving Element Method (3D MEM) and replaces the Timoshenko beam considered in earlier studies [2,3,7]. The 3D MEM avoids the moving vehicle exceeding the 'downstream' boundary end since this class of moving rail elements is attached to the vehicle. In fact, the vehicle remains fixed on a unique moving rail element instead of crossing from one element into another. This has two immediate and important consequences: firstly, there is no need to update the force or displacement vectors in the contact area because they are fixed on the same element; secondly, it permits to refine the mesh just around the fixed contact area, where forces and displacements are more pronounced. Both are hence important advantages in terms of computational cost compared to the FEM models commonly employed.

The 3D MEM formulation developed in Section 3 is utilised to compute numerically the resulting linear equation of motion, obtaining the element matrices and assembling them in global matrices by following the standard FE technique. These global matrices are not time dependent, and therefore they can be precalculated before the simulation starts and enable to adopt a modal approach. Using modal coordinates, the displacement vector of any point from the rail can be calculated through modal superposition. The number of modes calculated from the equation of motion is truncated to reduce the number of degrees of freedom of the governing system of differential equations and Newmark scheme is used to solve it at each time step.

ACCEPTED MANUSCRIPT

Regarding the wheelset, a flexible model negotiating a tangent track developed by Martínez-Casas *et al.* [3] is used. This model also takes into account the gyroscopic and inertial effects associated with the rotation by using Eulerian-modal coordinates, which reduce the dimension of the dynamic system and thus the computational cost. Only one single wheelset is incorporated instead of one complete bogie in order to simplify the computational problem, and forces are prescribed at the primary suspension seats, according to a procedure described in Section 2.1.

Results for the proposed modelling approach are presented and discussed for a selected vehicle type and a tangent track for different excitation sources including rail roughness and wheel flats. All the simulation cases are made for a Timoshenko beam and a 3D MEM rail model. Results with both rail models are compared focusing on the differences in the contact forces above the range of validity of the Timoshenko beam (from 1.5 kHz).

The paper is organised as follows: the vehicle-track interaction model is detailed in Section 2, where the flexible wheelset model, the Timoshenko beam track model and the contact coupling are discussed. Section 3 presents the complete formulation of the 3D MEM for a flexible track. Simulation results for different running conditions are presented in Section 4 and the paper closes with the conclusive remarks in Section 5.

2. THE VEHICLE-TRACK INTERACTION MODEL

For the vehicle-track interaction model, a substructuring technique [14,15] is followed in this paper, permitting to divide the whole system into three substructures (see Fig. 1): the vehicle, the rails and the rail supports. The equations of motion of each substructure are coupled by the wheel-rail contact forces and by the forces generated at the rail pads [14].

ACCEPTED MANUSCRIPT

The vehicle is confined to one wheelset with primary suspension. This has been modelled as a flexible and rotating wheelset [3] detailed in Section 2.1, in which Eulerian-modal coordinates are employed due to the axial symmetry of the body.

2.1. The vehicle model

The wheelset is mostly subjected to dynamic forces from the train-track interaction in a range above 20 Hz, in which short wavelength geometric imperfections in the wheel and rail profiles and singularities such as rail dips and wheelflats excite the vehicle. In this frequency range, the mechanical filter introduced by the suspensions effectively isolates the sprung masses (bogie frame and car body) from the motion of the un-sprung masses (wheelsets and axle boxes). Therefore, the vehicle is modelled through one single elastically flexible wheelset together with the primary suspension represented using viscoelastic lumped parameter elements. Two static forces on the primary suspensions are included to represent the weight of the bogie and the car body.

The flexible wheelset model negotiating a tangent track used in this work was previously developed by Martínez-Casas *et al.* [3]. Fig. 2 shows the axisymmetric mesh adopted. The model takes into account the gyroscopic and inertial effects associated with the rotation.

The coordinates that are implemented in the wheelset model do not follow the material points of the solid, but they are associated with spatial points (Eulerian approach). Any property of the solid $\varphi(\mathbf{u},t)$ corresponds to the material point whose undeformed configuration is in the spatial point $\mathbf{u}$ at instant *t*.

A modal approach is adopted, in which $\mathbf{\Phi}(\mathbf{u})$ is the mode shape function matrix of the free-boundary wheelset. This matrix does not depend on time since the rotation of the solid

ACCEPTED MANUSCRIPT

does not change the mode shape functions in fixed coordinates due to the axial symmetry of the wheelset. The use of the mode shapes in fixed coordinates as basis functions when the solid is in motion is called Eulerian-modal approach.

The modal properties are computed from a FE model, resulting the following modal equation of motion

$$\ddot{\mathbf{q}} + 2\Omega \boldsymbol{\Phi}_{FE}^{\mathrm{T}} \mathbf{V} \boldsymbol{\Phi}_{FE} \dot{\mathbf{q}} + \left(\mathbf{D} + \Omega^2 \boldsymbol{\Phi}_{FE}^{\mathrm{T}} (\mathbf{A} - \mathbf{C}) \boldsymbol{\Phi}_{FE} \right) \mathbf{q} = \Omega^2 \boldsymbol{\Phi}_{FE}^{\mathrm{T}} \mathbf{c} + \mathbf{Q} \tag{1}$$

$\mathbf{q}(t)$ being the modal coordinates, Ω the angular velocity of the wheelset, $\boldsymbol{\Phi}_{FE}$ the assembled mode shapes computed through the FE model, $\mathbf{D}$ a diagonal matrix that contains the squared undamped natural frequencies of the free-boundary solid and $\mathbf{Q}$ the generalized forces. The term containing $\mathbf{V}$ can be identified as an inertial force due to Coriolis acceleration associated with the convective velocity, $\mathbf{A}$ is related to convective acceleration, $\mathbf{C}$ is associated with centrifugal forces that appear after the deformation of the solid and $\mathbf{c}$ corresponds to constant centrifugal forces. These matrices are obtained for each element as

$$\mathbf{V}^e = \int_{Vol^e} \rho \mathbf{N}^{e\mathrm{T}} \left(\sum_i \tilde{u}_i \frac{\partial \mathbf{N}^e}{\partial u_i} \right) \mathrm{d}\upsilon \tag{2}$$

$$\mathbf{A}^e = \int_{Vol^e} \rho \mathbf{N}^{e\mathrm{T}} \left(\sum_j \sum_i \tilde{u}_i \tilde{u}_j \frac{\partial^2 \mathbf{N}^e}{\partial u_i \partial u_j} \right) \mathrm{d}\upsilon \tag{3}$$

$$\mathbf{C}^e = \int_{Vol^e} \rho \mathbf{N}^{e\mathrm{T}} \left(\sum_{i=1,3} u_i \frac{\partial \mathbf{N}^e}{\partial u_i} \right) \mathrm{d}\upsilon \tag{4}$$

$$\mathbf{c}^e = \int_{Vol^e} \rho \mathbf{N}^{e\mathrm{T}} \mathbf{E}\mathbf{u} \, \mathrm{d}\upsilon \tag{5}$$

ACCEPTED MANUSCRIPT

$\mathbf{N}^e(\mathbf{u})$ being the shape function matrix of the e-th element and $\mathbf{E} = \begin{pmatrix} 1 & 0 & 0 \\ 0 & 0 & 0 \\ 0 & 0 & 1 \end{pmatrix}$.

2.2. The track model

The track is included by two different flexible models in the present paper: a Timoshenko beam [11,14] with a limited frequency range of validity, and the 3D Moving Element Method (MEM) which enables to extend the range to the high frequency domain. The 3D MEM model will be formulated in detail in Section 3.

A cyclic approach [14] is considered in both cases since it provides some benefits with respect to classical track modelling. As seen in Fig. 3, according to this reference [14], the model can be interpreted as an infinite track negotiated by an infinite number of identical vehicles separated uniformly by a distance L and travels at the same velocity V. The constant distance L is set large enough to avoid the dynamic interaction between the vehicles and cyclic boundary conditions are introduced at the ends of the model (same displacements and their derivatives at the ends of the finite rail having length L). Hence, due to the periodicity of the structure and load conditions, the study of the track is reduced to a single section with finite length L.

Timoshenko beam was adopted in previous works [2,3,7] to model the rails. This model allows to include vertical/lateral bending and torsional deformations. Rail vibration is formulated as modal superposition for the unconstrained rail with cyclic boundary conditions, hence resulting into a set of decoupled 1-d.o.f. (degrees of freedom) equations. For a tangent track, only one single Timoshenko beam is considered to model the rail due to the symmetry of the track system with respect to its centreline.

ACCEPTED MANUSCRIPT

According to reference [1], for one single Timoshenko beam the frequency range of validity is up to 1.5 kHz for lateral rail vibration and up to 2 kHz for vertical vibration. In order to minimise errors due to modal truncation, the procedure presented in Ref. [14] was followed and rail modes up to 8.5 kHz were considered.

The sleepers are introduced as discrete rail supports as seen in Fig. 4. The rail pads are modelled as lumped viscoelastic elements connecting and, hence, coupling the rails and the sleepers, represented as lumped masses. Ballast dynamics are not relevant for the dynamic behaviour of the wheelset, and thus they have been replaced by an equivalent ballast stiffness and damping below the lumped masses.

2.3. The model of wheel-rail contact forces

The wheel-rail contact forces on the contact patch are the responsible of the coupling between the flexible wheelset and the track. These forces depend on the relative wheel-rail displacement and velocity in the contact area. Considering the same materials for both bodies, the tangential contact is coupled with the normal contact, but not vice versa. Hertzian model is adopted here for the normal contact and FASTSIM [16] is the software used for the tangential contact that depends on the normal contact force and creepages. Wheel-rail displacements and velocities are updated at each time step to evaluate the online contact forces.

3. 3D MOVING ELEMENT METHOD (3D MEM)

ACCEPTED MANUSCRIPT

ACCEPTED MANUSCRIPT

This section presents the effort of extending the 3D FEM to the MEM formulated by Koh *et al.* [12] in order to widen the frequency range of validity of the Timoshenko beam model used in previous works [2,3,7]. Both the MEM and the FEM need the following mathematical step:

$$\int_{\substack{solid\\volume}} f = \sum_{elements} \int_{\substack{element\\volume}} f \,, \tag{6}$$

As seen, the integral of the function f over the volume of the solid is the sum of the integrals over the finite element volume. This is correct if some conditions of continuity are satisfied. The MEM needs to compute the integral in Eq. (6) with f being the second derivative of the shape functions. In the proposed model, quadratic shape functions are used with C^0 continuity between elements. Thus, Eq. (6) can only be applied if the maximum order of differentiation is 1 [17], which means that integration by parts is necessary in the current formulation to obtain lower order derivatives. The present model solves this mathematical gap on the convective acceleration term which has not been treated in previous works.

The MEM was presented first in Ref. [12] through discretising a finite Euler-Bernoulli beam into 1D moving beam elements (conceptual elements attached to the moving vehicle that 'flow' with it). The present work extends the MEM to the 3D domain. A UIC60 profile is meshed and the 2D mesh generated is extruded longitudinally as seen in Fig. 5, which is out of scale. The finitely long rail mesh consists of 3D brick elements and the MEM is applied. Cyclic boundary conditions are adopted, which simulate the results of an infinite beam with a single load in the middle of the rail if the track length is sufficiently large and the displacements and their corresponding velocities at the edges are close to zero.

ACCEPTED MANUSCRIPT

A Cartesian coordinate system $x_1x_2x_3$ is adopted which moves with velocity V. An Eulerian position vector $\mathbf{u}$ defined through the coordinate system $x_1x_2x_3$ is considered. Vector $\mathbf{u}$ defines the position of a spatial point and it does not depend on time. Vector $\mathbf{w}=\mathbf{w}(\mathbf{u},t)$ is the displacement of a material point that occupies the position $\mathbf{u}$ at the instant t with respect the undeformed configuration. The position vector of the material point is

$$\mathbf{r}=\mathbf{u}+\mathbf{w}(\mathbf{u},t) \tag{7}$$

The cyclic boundary condition is satisfied if the displacements at the left edge of the model are equal to the ones of the right edge, that is

$$\mathbf{w}\left((0,u_2,u_3)^{\mathrm{T}},t\right)=\mathbf{w}\left((L,u_2,u_3)^{\mathrm{T}},t\right) \tag{8}$$

The velocity and acceleration of the material point are computed through the material derivative as follows

$$\mathbf{v}=\frac{D\mathbf{r}}{Dt}=\frac{\partial\mathbf{r}}{\partial t}-V\frac{\partial\mathbf{r}}{\partial x_1}=(V,0,0)^{\mathrm{T}}+\dot{\mathbf{w}}-V\frac{\partial\mathbf{w}}{\partial x_1}, \tag{9}$$

$$\mathbf{a}=\frac{D\mathbf{r}}{Dt}=\frac{\partial\mathbf{r}}{\partial t}-V\frac{\partial\mathbf{r}}{\partial x_1}=\ddot{\mathbf{w}}-2V\frac{\partial\dot{\mathbf{w}}}{\partial x_1}+V^2\frac{\partial^2\mathbf{w}}{\partial x_1^2} \tag{10}$$

The virtual work associated with the inertial forces is

$$\delta W=\int_{Vol}\rho\,\delta\mathbf{w}^{\mathrm{T}}\mathbf{a}\,\mathrm{d}\upsilon=\int_{Vol}\rho\,\delta\mathbf{w}^{\mathrm{T}}\ddot{\mathbf{w}}\,\mathrm{d}\upsilon-2V\int_{Vol}\rho\,\delta\mathbf{w}^{\mathrm{T}}\frac{\partial\dot{\mathbf{w}}}{\partial x_1}\,\mathrm{d}\upsilon+V^2\int_{Vol}\rho\,\delta\mathbf{w}^{\mathrm{T}}\frac{\partial^2\mathbf{w}}{\partial x_1^2}\,\mathrm{d}\upsilon \tag{11}$$

As mentioned above, the convergence of the last integral cannot be guaranteed due to third term of Eq. (11), $\int_{Vol}\rho\,\delta\mathbf{w}^{\mathrm{T}}\frac{\partial^2\mathbf{w}}{\partial x_1^2}\,\mathrm{d}\upsilon$, which contains a second derivative of the displacement vector,

and quadratic shape functions are used with C^0 continuity between elements. So, this term must be integrated by parts

$$\int_{Vol} \rho\, \delta\mathbf{w}^{\mathrm{T}} \frac{\partial^2 \mathbf{w}}{\partial x_1^2}\, \mathrm{d}x_1 \mathrm{d}x_2 \mathrm{d}x_3 = \int_{S} \rho\, \delta\mathbf{w}^{\mathrm{T}} \frac{\partial \mathbf{w}}{\partial x_1}\, \mathrm{d}x_2 \mathrm{d}x_3 - \int_{Vol} \rho\, \frac{\partial\left(\delta\mathbf{w}^{\mathrm{T}}\right)}{\partial x_1} \frac{\partial \mathbf{w}}{\partial x_1}\, \mathrm{d}x_1 \mathrm{d}x_2 \mathrm{d}x_3 \tag{12}$$

The surface integral is only computed over the lateral surfaces corresponding to the rail edges. A rail length L long enough to have negligible displacements at the model edges has been selected; thereby the integrand is close to zero and the influence of the surface integral can be neglected from a numerical point of view (this has been confirmed with a number of computational results that are not shown here for the sake of brevity). Hence, the convergence of Eq. (11) is guaranteed, resulting as

$$\delta W = \int_{Vol} \rho\, \delta\mathbf{w}^{\mathrm{T}} \ddot{\mathbf{w}}\, \mathrm{d}\upsilon - 2V \int_{Vol} \rho\, \delta\mathbf{w}^{\mathrm{T}} \frac{\partial \dot{\mathbf{w}}}{\partial x_1}\, \mathrm{d}\upsilon - V^2 \int_{Vol} \rho\, \frac{\partial\left(\delta\mathbf{w}^{\mathrm{T}}\right)}{\partial x_1} \frac{\partial \mathbf{w}}{\partial x_1}\, \mathrm{d}\upsilon \tag{13}$$

Now, the FE interpolation is adopted. The mesh is moving with $x_1 x_2 x_3$ frame and consequently the material of the rail flows into this mesh. The displacements in the volume of the e-th element Vol^e are computed by means of the shape functions as follows

$$\mathbf{w}(\mathbf{u}, t) = \mathbf{N}^e(\mathbf{u})\mathbf{w}^e(t) \qquad \text{if } \mathbf{u} \in Vol^e, \tag{14}$$

$\mathbf{w}^e$ being the nodal displacements. If Eq. (14) is implemented in Eq. (13), the following expression is obtained

$$\delta W = \sum_e \delta\mathbf{w}^{e\mathrm{T}} \left(\int_{Vol^e} \rho\, \mathbf{N}^{e\mathrm{T}} \mathbf{N}^e\, \mathrm{d}\upsilon\, \ddot{\mathbf{w}}^e - 2V \int_{Vol^e} \rho\, \mathbf{N}^{e\mathrm{T}} \frac{\partial \mathbf{N}^e}{\partial x_1}\, \mathrm{d}\upsilon\, \dot{\mathbf{w}}^e - V^2 \int_{Vol^e} \rho\, \frac{\partial \mathbf{N}^{e\mathrm{T}}}{\partial x_1} \frac{\partial \mathbf{N}^e}{\partial x_1}\, \mathrm{d}\upsilon\, \mathbf{w}^e \right) \tag{15}$$

ACCEPTED MANUSCRIPT

ACCEPTED MANUSCRIPT

The stiffness matrix $\mathbf{K}^e$ is the standard one because the potential energy associated with the elastic deflection does not distinguish between the Eulerian and the Lagrangian coordinates. Consequently, the equation of motion is

$$\mathbf{M}^e\ddot{\mathbf{w}}_G - 2V\,\mathbf{C}^e\dot{\mathbf{w}}_G + \left(\mathbf{K}^e - V^2\mathbf{A}^e\right)\mathbf{w}_G = \mathbf{F}^e, \tag{16}$$

where the corresponding element matrices are the following:

$$\mathbf{M}^e = \int_{Vol^e} \rho\,\mathbf{N}^{e\mathrm{T}}\mathbf{N}^e\,\mathrm{d}\upsilon \tag{17}$$

$$\mathbf{C}^e = \int_{Vol^e} \rho\,\mathbf{N}^{e\mathrm{T}}\frac{\partial\mathbf{N}^e}{\partial x_1}\,\mathrm{d}\upsilon \tag{18}$$

$$\mathbf{A}^e = \int_{Vol^e} \rho\,\frac{\partial\mathbf{N}^{e\mathrm{T}}}{\partial x_1}\frac{\partial\mathbf{N}^e}{\partial x_1}\,\mathrm{d}\upsilon \tag{19}$$

Matrix $\mathbf{C}^e$ is associated with the inertial force due to the convective velocity, $\mathbf{A}^e$ is related to the convective acceleration, and $\mathbf{F}^e$ is the force vector which contains the rail pad forces as well as the contact normal and tangential forces from the wheel-rail interaction applied on the head of the rail in its middle longitudinal position. Nodal coordinates are implemented in a global displacement vector $\mathbf{w}$, obtaining the global matrices $\mathbf{M}$, $\mathbf{C}$, $\mathbf{A}$, $\mathbf{K}$ and the global vector $\mathbf{F}$.

A modal approach is adopted at this point, so that the global displacement vector $\mathbf{w}$ can be expressed through superposition of mode shapes:

$$\mathbf{w}(\mathbf{u},t) = \boldsymbol{\Phi}(\mathbf{u})\,\mathbf{q}(t), \tag{20}$$

ACCEPTED MANUSCRIPT

where $\mathbf{\Phi}(\mathbf{u})$ is the mode shape function matrix of the cyclic boundary rail and $\mathbf{q}(t)$ is the modal coordinate vector. Matrix $\mathbf{\Phi}$ is built solving the eigenproblem from the global standard matrices $\mathbf{M}$ and $\mathbf{K}$. Since these matrices are symmetric, $\mathbf{\Phi}$ is orthogonal ($\mathbf{\Phi}^{-1} = \mathbf{\Phi}^{\mathrm{T}}$). The small rigid body displacements of the solid are considered through the rigid body modes of the rail. It must be pointed out that the mode shape functions do not depend on time since the 'flow' of the mesh through the material coordinates does not change the mode shape functions in spatial coordinates, because the cross-sectional area remains invariable after the extrusion of the profile.

Once the modal transform of Eq. (20) is applied in Eq. (16), the resulting equation is pre-multiplied by $\mathbf{\Phi}^{\mathrm{T}}$. The modal equation of motion results as

$$\tilde{\mathbf{M}}\ddot{\mathbf{q}} - 2V\,\tilde{\mathbf{C}}\dot{\mathbf{q}} + \left(\tilde{\mathbf{K}} - V^2\tilde{\mathbf{A}}\right)\mathbf{q} = \mathbf{\Phi}^{\mathrm{T}}\mathbf{F}\,, \tag{21}$$

where the modal matrices are calculated from the global matrices as follows:

$$\tilde{\mathbf{M}} = \mathbf{\Phi}^{\mathrm{T}}\mathbf{M}\mathbf{\Phi} = \begin{bmatrix} m_{rr} & 0 \\ 0 & \ddots \end{bmatrix} \tag{22}$$

$$\tilde{\mathbf{K}} = \mathbf{\Phi}^{\mathrm{T}}\mathbf{K}\mathbf{\Phi} = \begin{bmatrix} k_{rr} & 0 \\ 0 & \ddots \end{bmatrix} = \begin{bmatrix} \omega_r^2 m_{rr} & 0 \\ 0 & \ddots \end{bmatrix} \tag{23}$$

$$\tilde{\mathbf{C}} = \mathbf{\Phi}^{\mathrm{T}}\mathbf{C}\mathbf{\Phi} \tag{24}$$

$$\tilde{\mathbf{A}} = \mathbf{\Phi}^{\mathrm{T}}\mathbf{A}\mathbf{\Phi} \tag{25}$$

ω_r being the undamped natural frequencies. Since matrix $\mathbf{\Phi}$ is orthogonal, it diagonalises $\tilde{\mathbf{M}}$ and $\tilde{\mathbf{K}}$, while $\tilde{\mathbf{C}}$ and $\tilde{\mathbf{A}}$ are not diagonalised, thus the equation of motion is not uncoupled.

ACCEPTED MANUSCRIPT

For the simulations carried out, 900 vibration modes of each rail have been considered, covering a frequency range up to 8.5 kHz. As recommended in the literature [1], a damping loss factor $\zeta = 0.01$ is introduced in the rail. Therefore, a new modal damping matrix is included in the modal equation of motion as a diagonal matrix:

$$\tilde{\mathbf{C}}_{\zeta} = \begin{bmatrix} c_{rr} & 0 \\ 0 & \ddots \end{bmatrix} = 2\zeta \begin{bmatrix} \omega_r m_{rr} & 0 \\ 0 & \ddots \end{bmatrix} \tag{26}$$

Hence, the modal equation of motion is

$$\tilde{\mathbf{M}}\ddot{\mathbf{q}} + \left(\tilde{\mathbf{C}}_{\zeta} - 2V\,\tilde{\mathbf{C}}\dot{\mathbf{q}}\right) + \left(\tilde{\mathbf{K}} - V^2\tilde{\mathbf{A}}\right)\mathbf{q} = \mathbf{\Phi}^{\mathrm{T}}\mathbf{F}, \tag{27}$$

Eq. (27) is a linear second-order differential equation and then the matrices are calculated only once at the beginning of the simulation.

4. RESULTS

This section presents results for the proposed wheelset-track modelling approach when excited by random rail roughness and wheelflat. All the simulations consider the vehicle running at 300 km/h through a tangent track and the system is excited up to 8.5 kHz. Each case is run separately for a Timoshenko beam and a 3D MEM modelling the track. Both models are compared by the vertical and lateral contact forces obtained from the simulations above the range of validity of the Timoshenko beam (from 1.5 to 8.5 kHz) in order to study the contributions of the 3D MEM in the high frequency range. Finally, the pseudo-static deformation of the finitely long rail supported on a viscoelastic Winkler bedding is obtained

ACCEPTED MANUSCRIPT

using the 1D MEM model from Koh *et al.* [12] and the implemented 3D MEM. Results are shown for different speeds of the moving load.

The case studied here refers to the trailed car of a concentrated power train for high speed passenger service. The vehicle is equipped with a solid axle wheelset with monobloc, light design wheels. The track considered features UIC60 rails and track parameters are based on the EUROBALT project [18], considering a "stiff" track. Table 1 summarises the input data used to set up the simulation model.

Figs. 6 and 7 show the time history of the vertical and lateral contact forces respectively for excitation caused by randomly corrugated rails, assuming a corrugation spectrum corresponding to the ISO 3095 limit [19], which establishes a third-octave band spectrum of the rail roughness. As expected, the dynamic fluctuations of the vertical and lateral contact forces show a complex waveform, arising from the dynamic response of the wheelset-track system to broadband random excitation. The results for both track models present a similar trend and mean values, although a higher frequency content is observed for the 3D MEM in the vertical contact force.

An alternative plot for the wheel-rail contact force is depicted in the frequency domain. Fig. 8 represents the third-octave band spectrum of the vertical contact forces. There appear peaks in the antiresonances of the track frequency between the P2 and pinned-pinned frequencies in the 100-300 Hz band, and also in the band between 900 and 1400 Hz, whereas the smaller responses are at the P2 frequency (below 100 Hz), pinned-pinned frequency (below 1 kHz) and at a resonance frequency below 3 kHz. It can be observed that the Timoshenko beam shows greater vertical contact forces in the low and medium frequency range (up to 1 kHz, range of validity for the Timoshenko beam) due to the fact that Timoshenko model has greater stiffness than the 3D MEM model, since the straight section of the Timoshenko beam cannot be

ACCEPTED MANUSCRIPT

deformed. On the other hand, 3D MEM shows higher frequency content for higher frequencies (1-8.5 kHz band). These higher harmonics seem to be crucial to describe the high frequency phenomena, such as rolling and squeal noise.

Figs. 9 and 10 show the time history of the vertical and lateral contact forces with both rail models caused by a wheelflat when the wheelset runs over a perfectly even tangent track. In the simulations, a rounded geometry of the wheel flat with size 0.05 m is adopted. Intense dynamic effects are observed in both contact forces, initially leading to the occurrence of full loss of contact in the wheels, then followed by a severe impact causing peaks, and finally by a transient vibration that generates further dynamic fluctuations in all the force components. Results for both track models present again similar trends and mean values, the differences between both models being small in terms of duration of the contact loss. The maximum value of the vertical contact force, however, is larger when the 3D MEM is used. These results may indicate vertical contact forces will cause accelerated damage and degradation of the contacting surfaces as well as increased noise and vibration. The first overloading for this model is about 265% of the steady-state load, being 250% for the Timoshenko beam. For the second overloading, the 3D MEM reaches 210% of the steady-state load, while Timoshenko approach yields 170%. Finally, a higher frequency content in vertical contact force with the 3D MEM model is observed.

Fig. 11 represents the third-octave band spectrum of the vertical contact forces caused by a wheelflat. It can be observed that the Timoshenko beam model shows a slightly higher vertical contact force in low-medium frequency range up to 450 Hz, but the 3D MEM reveals a markedly content for higher frequencies (450 Hz - 8.5 kHz band). The results depicted in Fig. 11 are consistent with the previous figure in time domain, concluding that the 3D MEM describes the high frequency dynamics more accurately than the Timoshenko model.

ACCEPTED MANUSCRIPT

The effect of the vehicle speed on the 3D MEM has been evaluated for the pseudo-static deformation of the rail supported on a viscoelastic Winkler bedding with a stiffness per unit length of 10^7 N/m^2 and a damping per unit length of 4900 Ns/ m^2 [12]. The 'pseudo' prefix is added because it cannot be considered a static case since there is a load moving along the rail. For the Eulerian approach taken, the load is fixed in a spatial point while its corresponding speed is introduced in the formulation. For this purpose, the centreline of the rail has been selected to represent the deformation. Fig. 12a) shows a negligible influence for the Winkler foundation used, in agreement with Thompson [1]. The pseudo-static deformation for 150 km/h has been compared with the results given by the original 1D MEM from Koh *et al.* [12], which has been implemented for this purpose. This model is based on an Euler-Bernoulli beam discretised in *N* nodes, each one having the vertical displacement and rotation as degrees of freedom. Shape functions for 1D beam elements are used in order to apply the FE technique. Fig. 12b) shows a good agreement between both models, with a discrepancy of 3% at the contact point.

5. CONCLUSIONS

This paper has presented a new 3D model for a finitely long railway track which has been formulated through the MEM and developed as a FE approach in order to improve the modelling of the high frequency dynamics. The model considers an Eulerian coordinate system attached to the moving vehicle instead of a fixed coordinate system and adopts cyclic boundary conditions. This approach permits to decrease the computational cost compared to the FE models commonly used.

Results for the vertical and lateral contact forces are presented for two types of excitation: randomly corrugated tangent track and excitation arising from a wheelflat when the wheelset

ACCEPTED MANUSCRIPT

runs over a perfectly even track at 300 km/h. The 3D MEM and Timoshenko beam have been compared in all the simulations. Both models show a similar behaviour in the low and mid frequency domain for two excitation cases, where similar trends and mean values are observed.

In the randomly corrugated track case considered, the Timoshenko beam model shows a larger vertical contact force in low and mid frequency range up to 1 kHz (range of validity for the Timoshenko beam), but the 3D MEM shows a higher frequency content for the 1-8.5 kHz band. These higher harmonics seem to be crucial to describe the high frequency phenomena, such as rolling and squeal noise.

For wheelflat excitation, the first and second overloading of the vertical contact force using 3D MEM are larger than those obtained with the Timoshenko beam model. Therefore, it may be expected to cause accelerated damage and degradation of the contacting surfaces as well as increased noise and vibration. In frequency domain, the Timoshenko beam shows slightly greater vertical contact forces in low and mid frequency range up to 450 Hz, but 3D MEM model shows a remarkably higher frequency content in the 450 Hz - 8.5 kHz band.

The pseudo-static deformation of the rail supported on a viscoelastic foundation has been compared to the 3D MEM and 1D (Euler-Bernoulli beam) MEM models. Both results practically overlap with a maximum discrepancy of 3% at the contact point. The speed of the moving load does not have a significant influence on the solution.

Finally, these results validate the 3D MEM as an efficient flexible track model whereas it reproduces consistently the contrasted behaviour of the Timoshenko beam for its range of validity according to the literature. It is concluded that the proposed 3D MEM track model seems to be suitable to describe the high frequency dynamics associated with different railway phenomena such as short pitch rail corrugation, wheelflat excitation, axle fatigue, rolling, squeal and braking noise.

ACCEPTED MANUSCRIPT

ACKNOWLEDGEMENTS

The authors gratefully acknowledge the financial support of Ministerio de Economía y Competitividad and the European Regional Development Fund (project TRA2013-45596-C2-1-R), as well as Generalitat Valenciana (project Prometeo/2012/023) and Ministerio de Educación, Cultura y Deporte (project SP20140659) as part of Programa Campus de Excelencia Internacional.

REFERENCES

[1] D. J. Thompson, *Railway Noise and Vibration: Mechanisms, Modelling and Means of Control*, Elsevier, 2009.

[2] P. Vila, L. Baeza, J. Martínez-Casas, J. Carballeira, *Rail corrugation growth accounting for the flexibility and rotation of the wheelset and the non-Hertzian and non-steady state effects at contact patch*, Vehicle System Dynamics 52 (Supplement 1) (2014) 92-108.

[3] J. Martínez-Casas, L. Mazzola, L. Baeza, S. Bruni, *Numerical estimation of stresses in railway axles using a train-track interaction model*, International Journal of Fatigue 47 (2013) 18-30.

[4] K. Popp, I. Kaiser, *Interaction of elastic wheelsets and elastic rails: modelling and simulation*, Vehicle System Dynamics 44 (Suppl.) (2006) S932-S939.

[5] D. J. Thompson, C. J. C. Jones, *A Review of the Modelling of Wheel/Rail Noise Generation*, Journal of Sound and Vibration 231 (3) (2000) 519-536.

ACCEPTED MANUSCRIPT

[6] I. Kaiser, *Refining the modelling of vehicle-track interaction*, Vehicle System Dynamics 50 (Suppl.) (2012) S229-S243.

[7] J. Martínez-Casas, E. Di Gialleonardo, S. Bruni, L. Baeza, *A comprehensive model of the railway wheelset-track interaction in curves*, Journal of Sound and Vibration 333 (2014) 4152-4169.

[8] P. M. Mathews, *Vibrations of a beam on elastic foundation*, Zeitschrift für Angewandte Mathematik und Mechanik 38 (1958) 105 -115.

[9] P. M. Mathews, *Vibrations of a beam on elastic foundation II*, Zeitschrift für Angewandte Mathematik und Mechanik 39 (1959) 13-19.

[10] L. Jézéquel, *Response of periodic systems to a moving load*, Journal of Applied Mechanics (ASME) 48 (1981) 613- 618.

[11] S. Timoshenko, D. H. Young, W. Weaver Jr., *Vibration Problems in Engineering* (4th edn), John Wiley: New York, 1974.

[12] C. G. Koh, J. S. Y. Ong, D. K. H. Chua, J. Feng, *Moving Element Method for train-track dynamics*, International Journal for Numerical Methods in Engineering 56 (2003) 1549-1567.

[13] C. G. Koh, G. H. Chiew, C. C. Lim, *A numerical method for moving load on continuum*, Journal of Sound and Vibration 300 (2007) 126-138.

[14] L. Baeza, H. Ouyang, *A railway track dynamics model based on modal substructuring and cyclic boundary condition*, Journal of Sound and Vibration 330 (2011) 75-86.

[15] L. Baeza, A. Roda, J. C. O. Nielsen, *Railway vehicle/track interaction analysis using a modal substructuring approach*, Journal of Sound and Vibration 293 (2006) 112-124.

ACCEPTED MANUSCRIPT

[16] J. J. Kalker, *A fast algorithm for the simplified theory of rolling contact*, Vehicle System Dynamics 11 (1982) 1-13.

[17] O. C. Zienkiewicz, R. L. Taylor, J. Z. Zhu, *The finite element method: Its basis and fundamentals*, Elsevier Butterworth-Heinemann, 2005.

[18] L. Mazzola, Y. Bezin, S. Bruni, *Vehicle-Track interaction: MB simulation for track loading limits and damage identification*, ECCOMAS Thematic Conference Multibody Dynamics 2011, Brussels, Belgium.

[19] ISO 3095:2013, *Acoustics. Railway applications. Measurement of noise emitted by railbound vehicles*.

ACCEPTED MANUSCRIPT

ACCEPTED MANUSCRIPT

FIGURE CAPTIONS

Fig. 1. Scheme of the vehicle-track interaction model.

Fig. 2. Finite element mesh of the flexible wheelset.

Fig. 3. Cyclic track model.

Fig. 4. Details of the track model. Left: sleeper bays. Right: sleeper and rail pad.

Fig. 5. Finite element mesh of the flexible rail.

Fig. 6. Vertical wheel-rail contact forces when the vehicle circulates at 300 km/h speed on a randomly corrugated tangent track. Amplitudes corresponding to the ISO 3095 limit.

Fig. 7. Lateral wheel-rail contact forces when the vehicle circulates at 300 km/h speed on a randomly corrugated tangent track. Amplitudes corresponding to the ISO 3095 limit.

Fig. 8. Frequency domain plot of the vertical wheel-rail contact forces when the vehicle circulates at 300 km/h speed on a randomly corrugated tangent track. Amplitudes corresponding to the ISO 3095 limit.

Fig. 9. Vertical wheel-rail contact forces when the vehicle circulates at 300 km/h speed on a perfectly even tangent track in presence of a 0.05 m wheelflat.

Fig. 10. Lateral wheel-rail contact forces when the vehicle circulates at 300 km/h speed on a perfectly even tangent track in presence of a 0.05 m wheelflat.

Fig. 11. Frequency domain plot of the vertical wheel-rail contact forces when the vehicle circulates at 300 km/h speed on a perfectly even tangent track in presence of a 0.05 m wheelflat.

ACCEPTED MANUSCRIPT

Fig. 12. Pseudo-static deformation of the finitely long rail supported on a viscoelastic foundation: a) different moving load speeds; b) different MEM models for V = 150 km/h.

ACCEPTED MANUSCRIPT

ACCEPTED MANUSCRIPT

TABLE CAPTIONS

Table 1. Simulation parameters and properties.

ACCEPTED MANUSCRIPT

Figure01

ACCEPTED MANUSCRIPT

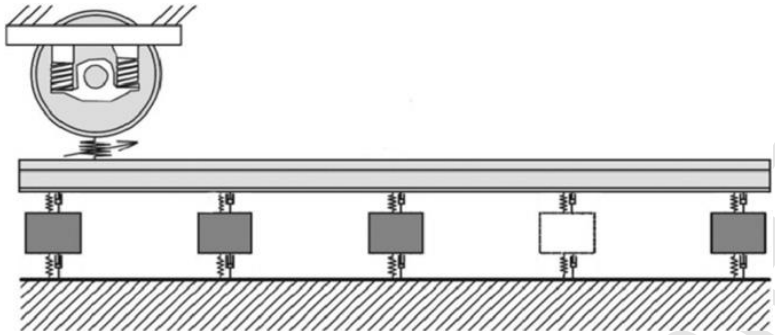

Fig. 1. Scheme of the vehicle-track interaction model.

ACCEPTED MANUSCRIPT

Figure02

ACCEPTED MANUSCRIPT

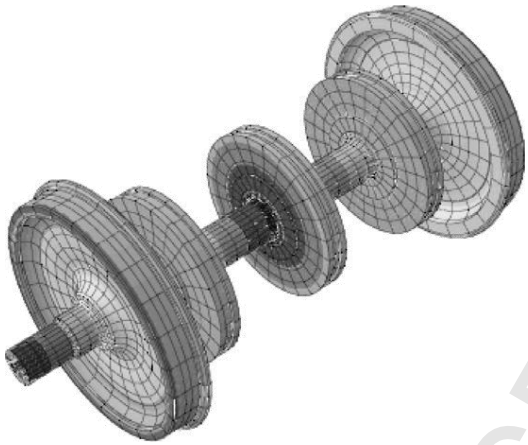

Fig. 2. Finite element mesh of the flexible wheelset.

ACCEPTED MANUSCRIPT

Figure03

ACCEPTED MANUSCRIPT

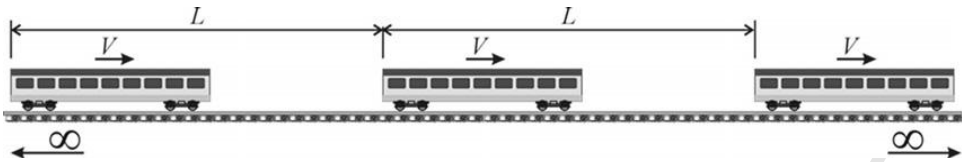

Fig. 3. Cyclic track model.

ACCEPTED MANUSCRIPT

ACCEPTED MANUSCRIPT

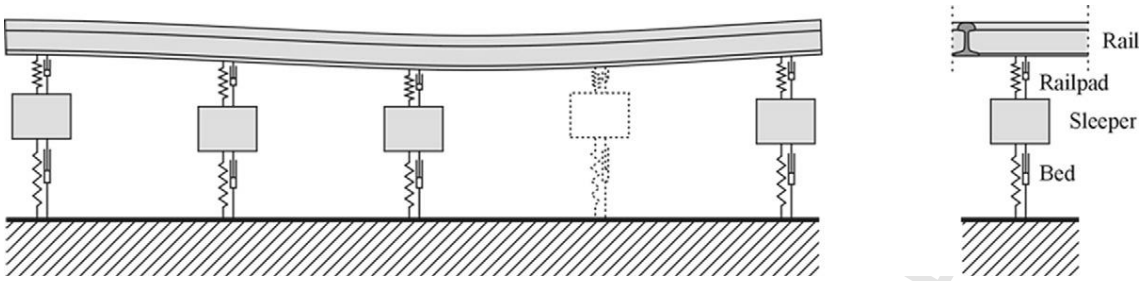

Fig. 4. Details of the track model. Left: sleeper bays. Right: sleeper and rail pad.

ACCEPTED MANUSCRIPT

Figure05

ACCEPTED MANUSCRIPT

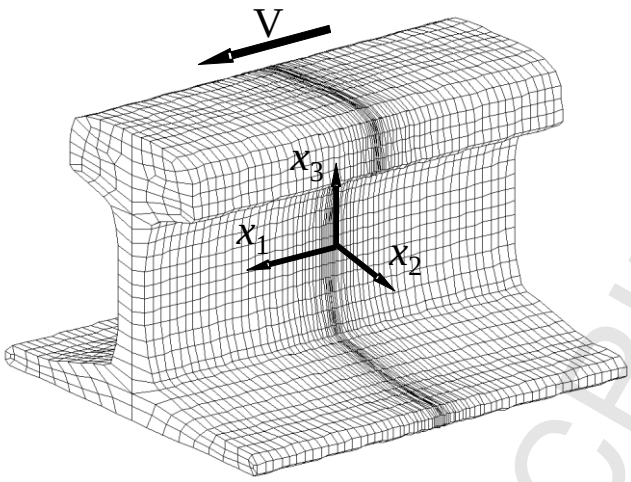

Fig. 5. Finite element mesh of the flexible rail.

ACCEPTED MANUSCRIPT

Figure06 revised

ACCEPTED MANUSCRIPT

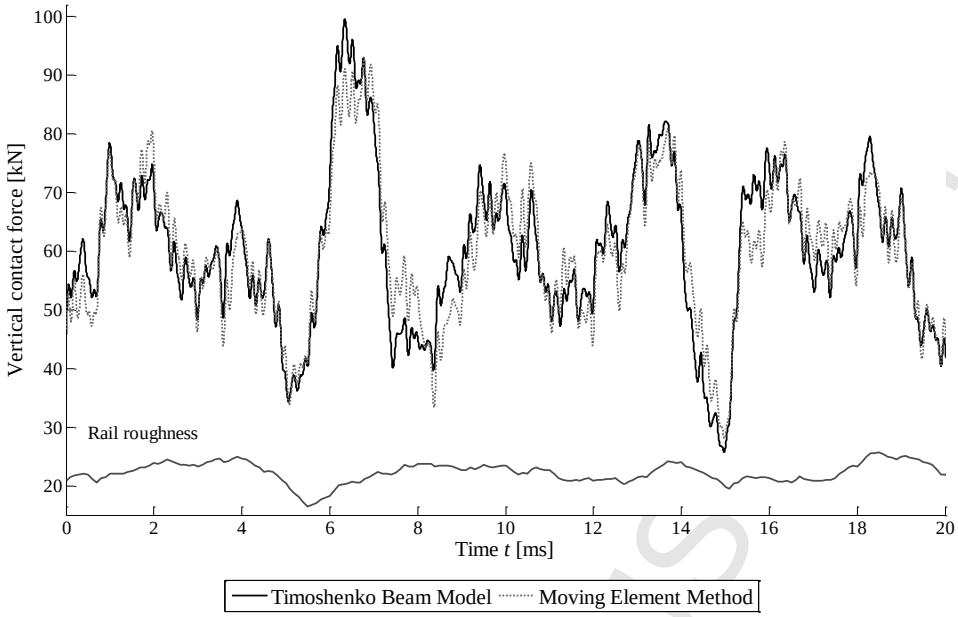

Fig. 6. Vertical wheel-rail contact forces when the vehicle circulates at 300 km/h speed on a randomly corrugated tangent track. Amplitudes corresponding to the ISO 3095 limit.

ACCEPTED MANUSCRIPT

Figure07 revised

ACCEPTED MANUSCRIPT

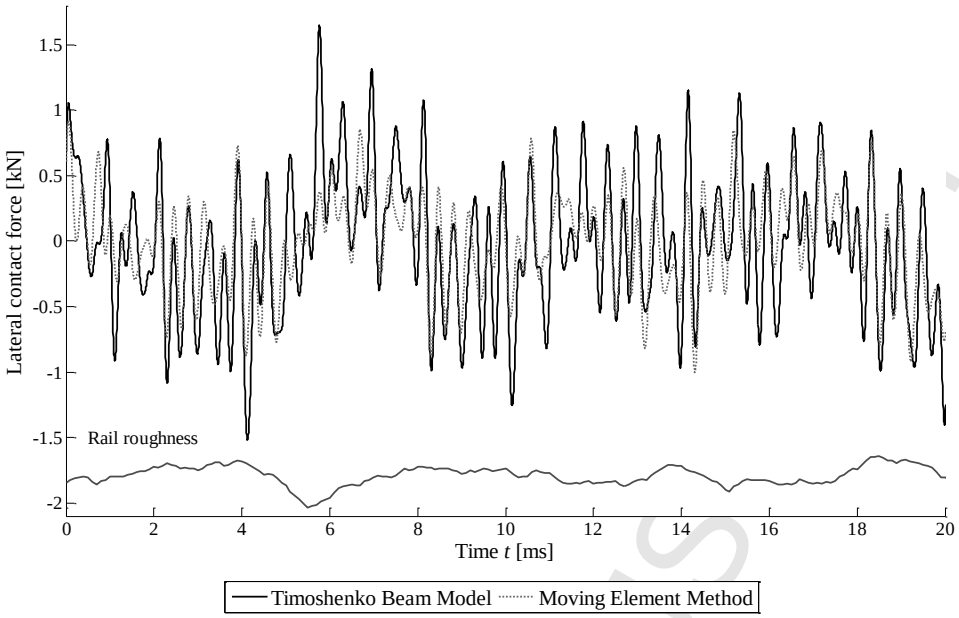

Fig. 7. Lateral wheel-rail contact forces when the vehicle circulates at 300 km/h speed on a randomly corrugated tangent track. Amplitudes corresponding to the ISO 3095 limit.

ACCEPTED MANUSCRIPT

Figure08 revised

ACCEPTED MANUSCRIPT

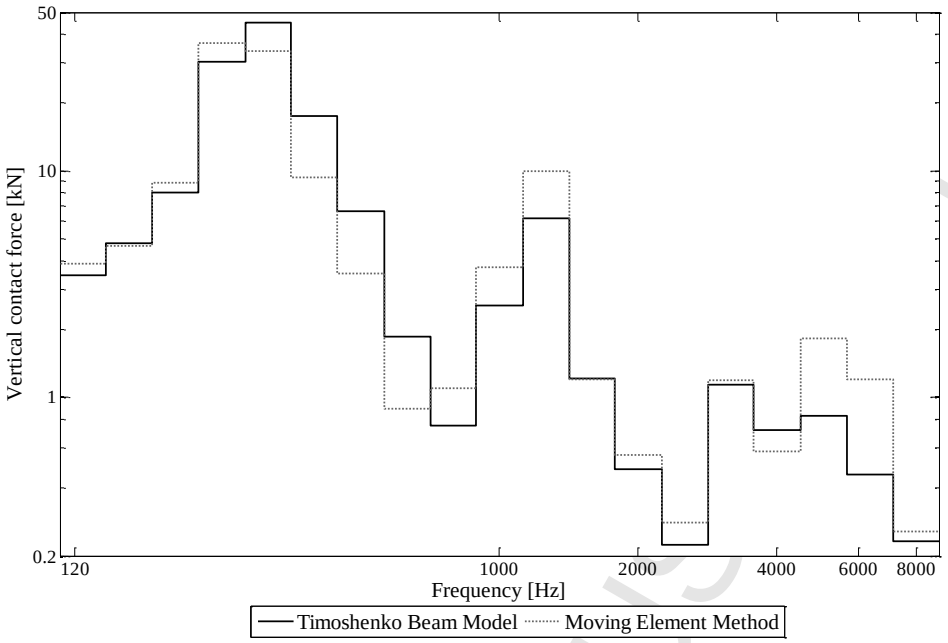

Fig. 8. Frequency domain plot of the vertical wheel-rail contact forces when the vehicle circulates at 300 km/h speed on a randomly corrugated tangent track. Amplitudes corresponding to the ISO 3095 limit.

ACCEPTED MANUSCRIPT

ACCEPTED MANUSCRIPT

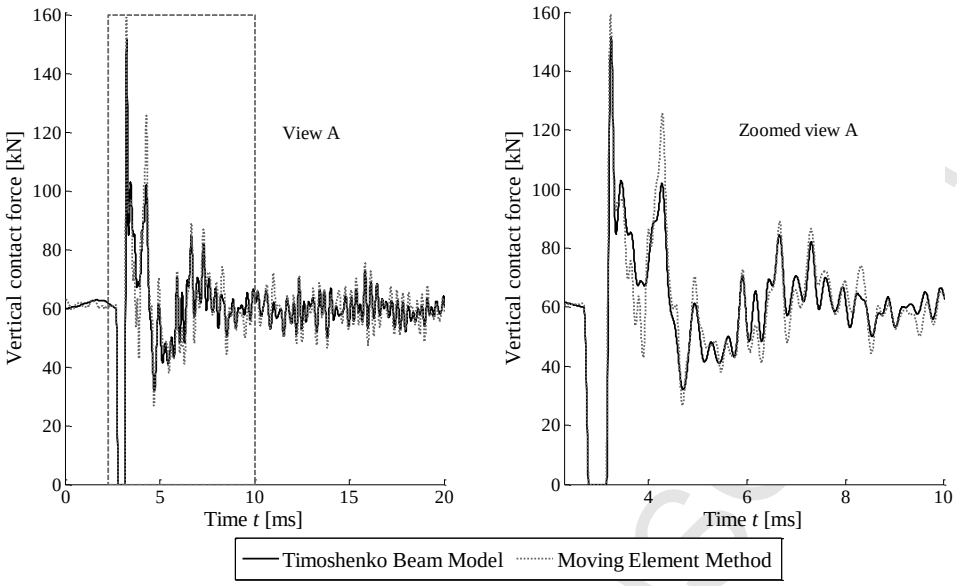

Fig. 9. Vertical wheel-rail contact forces when the vehicle circulates at 300 km/h speed on a perfectly even tangent track in presence of a 0.05 m wheelflat.

ACCEPTED MANUSCRIPT

Figure10 revised

ACCEPTED MANUSCRIPT

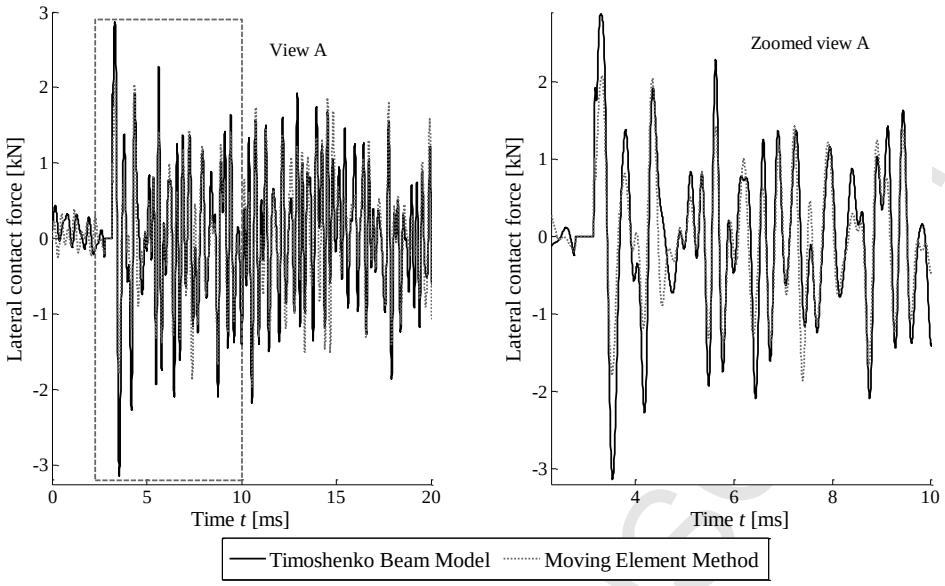

Fig. 10. Lateral wheel-rail contact forces when the vehicle circulates at 300 km/h speed on a perfectly even tangent track in presence of a 0.05 m wheelflat.

ACCEPTED MANUSCRIPT

ACCEPTED MANUSCRIPT

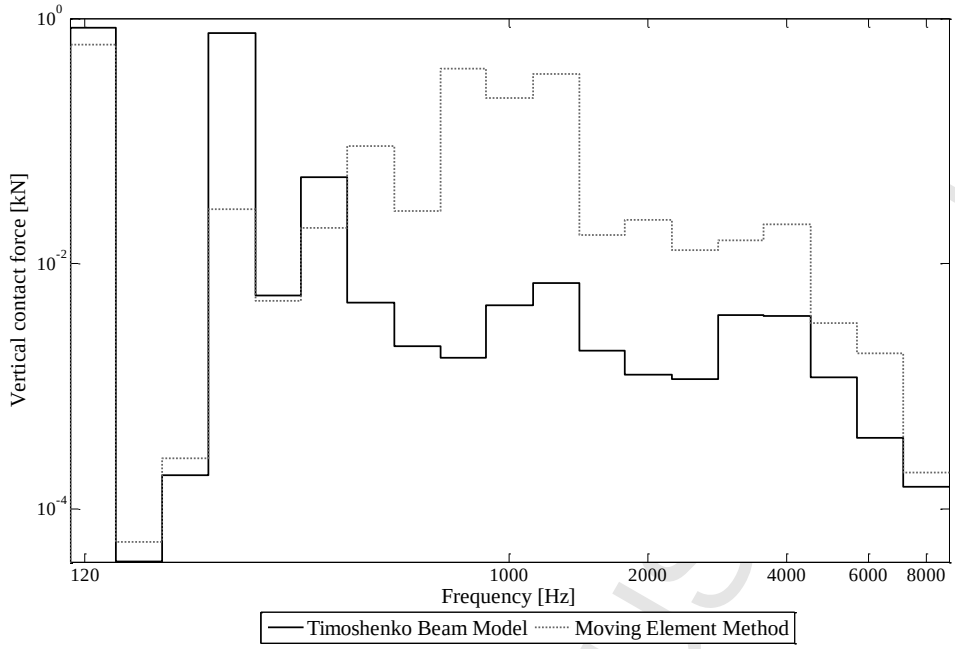

Fig. 11. Frequency domain plot of the vertical wheel-rail contact forces when the vehicle circulates at 300 km/h speed on a perfectly even tangent track in presence of a 0.05 m wheelflat.

ACCEPTED MANUSCRIPT

Figure12

ACCEPTED MANUSCRIPT

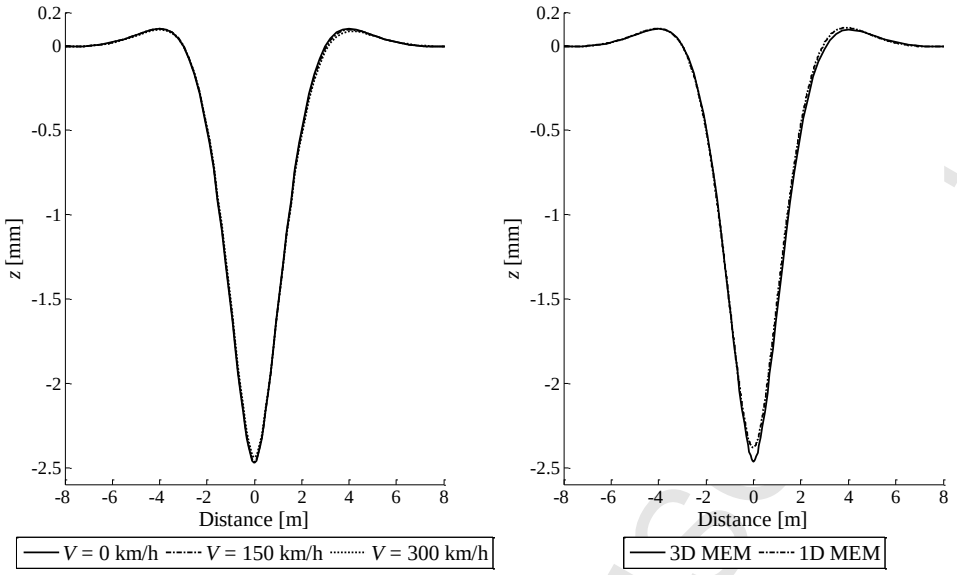

Fig. 12. Pseudo-static deformation of the finitely long rail supported on a viscoelastic foundation: a) different moving load speeds; b) different MEM models for V = 150 km/h.

ACCEPTED MANUSCRIPT

Table01

ACCEPTED MANUSCRIPT

Wheelset model data		**Track model data**	
Mass of wheelset	1375 kg	Sleeper bay	0.6 m
Axle load	120 kN	Sleeper number	70
Primary suspension longitudinal stiffness	7.5 MN/m	Sleeper mass	324 kg
Primary suspension lateral stiffness	7.1 MN/m	Track bed stiffness	200 MN/m
Primary suspension vertical stiffness	0.81 MN/m	Track bed damping	150 kN s/m
Primary suspension longitudinal damping	100 kN s/m	Rail pad stiffness	1 GN/m
Primary suspension lateral damping	100 kN s/m	Rail pad damping	50 kN s/m
Primary suspension vertical damping	30 kN s/m	Rail section	UIC60

Table 1. Simulation parameters and properties.

ACCEPTED MANUSCRIPT

ACCEPTED MANUSCRIPT

Captions are :

- Figure06_Revised.fig : "Fig. 6. Vertical wheel-rail contact forces when the vehicle circulates at 300 km/h speed on a randomly corrugated tangent track. Amplitudes corresponding to the ISO 3095 limit."

- Figure07_Revised.fig : "Fig. 7. Lateral wheel-rail contact forces when the vehicle circulates at 300 km/h speed on a randomly corrugated tangent track. Amplitudes corresponding to the ISO 3095 limit."

- Figure08_Revised.fig : "Fig. 8. Frequency domain plot of the vertical wheel-rail contact forces when the vehicle circulates at 300 km/h speed on a randomly corrugated tangent track. Amplitudes corresponding to the ISO 3095 limit."

- Figure09_Revised.fig : "Fig. 9. Vertical wheel-rail contact forces when the vehicle circulates at 300 km/h speed on a perfectly even tangent track in presence of a 0.05 m wheelflat."

- Figure10_Revised.fig : "Fig. 10. Lateral wheel-rail contact forces when the vehicle circulates at 300 km/h speed on a perfectly even tangent track in presence of a 0.05 m wheelflat."

- Figure11_Revised.fig : "Fig. 11. Frequency domain plot of the vertical wheel-rail contact forces when the vehicle circulates at 300 km/h speed on a perfectly even tangent track in presence of a 0.05 m wheelflat."

- Figure12.fig : "Fig. 12. Pseudo-static deformation of the finitely long rail supported on a viscoelastic foundation: a) different moving load speeds; b) different MEM models for V = 150 km/h."

ACCEPTED MANUSCRIPT